Efficient organic room-temperature phosphorescence in both solution and solid states

Chensen Li[1,2,9], Zhenchen Lou[3,9], Minghui Wu[4,9], Xinmeng Chen[1], Haozhe Tan[2], Zonghang Liu[2], Feng Gao[2], Zijie Qiu[2], Zheng Zhao*[2], Lianrui Hu*[3], Guohua Xie*[5], Maoqiu Li[6], Yumeng Guo[6], Zhongjie Ren*[6], Song Zhang[7], Yuchao Liu[8], Shouke Yan[6,8], Ryan T. K. Kwok[1], Jacky W. Y. Lam[1], Ben Zhong Tang*[1,2]

1. *Department of Chemistry and Hong Kong Branch of Chinese National Engineering Research Center for Tissue Restoration and Reconstruction, The Hong Kong University of Science and Technology, Kowloon, Hong Kong, China.*
2. *School of Science and Engineering, Shenzhen Institute of Aggregate Science and Technology, The Chinese University of Hong Kong, Shenzhen (CUHK-Shenzhen), Guangdong 518172, China.*
3. *Shanghai Key Laboratory of Green Chemistry and Chemical Processes, Shanghai Frontiers Science Center of Molecule Intelligent Syntheses, School of Chemistry and Molecular Engineering, East China Normal University, 3663 N. Zhongshan Road, Shanghai 200062, China.*
4. *Department of Chemistry, Southern University of Science and Technology, Shenzhen 518055, China.*
5. *The Institute of Flexible Electronics (Future Technologies), Xiamen University, Xiamen 361005, China.*
6. *State Key Laboratory of Chemical Resource Engineering, College of Materials Science and Engineering, Beijing University of Chemical Technology, Beijing 100029, China.*
7. *State Key Laboratory of Magnetic Resonance and Atomic and Molecular Physics, Wuhan Institute of Physics and Mathematics, Chinese Academy of Sciences, Wuhan 430071, China.*
8. *Key Laboratory of Rubber-Plastics, Ministry of Education, Qingdao University of Science & Technology, Qingdao, 266042, China.*
9. *These authors contributed equally: Chensen Li, Zhenchen Lou, Minghui Wu.*

https://doi.org/10.26434/chemrxiv-2024-hqwbs **ORCID:** https://orcid.org/0009-0009-6810-7086 Content not peer-reviewed by ChemRxiv. **License:** CC BY 4.0

Corresponding emails: zhaozheng@cuhk.edu.cn (Zheng Zhao); lrhu@chem.ecnu.edu.cn (Lianrui Hu); ifeghxie@xmu.edu.cn (Guohua Xie); renzj@mail.buct.edu.cn (Zhongjie Ren); tangbenz@cuhk.edu.cn (Ben Zhong Tang)

Abstract: Organic room-temperature phosphorescence (RTP) materials possess immense potential for a variety of applications. However, conventional RTP materials face substantial problems, such as no phosphorescence in ambient solution, and inefficient amorphous films and electroluminescence devices. To address these issues, intrinsic RTP emitters can display efficient RTP in various states and achieve multiple desired properties through the same molecule. In this work, dendrimers are first used to design of efficient intrinsic RTP materials by incorporating dendrons as triplet regulators to facilitate effective spin-orbit coupling, intersystem crossing, and triplet radiative transitions that exhibit a significant transformation from delayed fluorescence to intrinsic RTP in different states. The dendrimers exhibit long phosphorescence lifetime within milliseconds in ambient solution, photoluminescence quantum yield of 98% in doped films, and substantially high external quantum efficiency of 25.1% in the organic electroluminescence devices. Moreover, by regulating the triplet characteristics of the dendrimers, the dendrimers display up-converted anti-Kasha dual-RTP emissions and an ultra-long afterglow lifetime within seconds in rigid polymer matrixes. These results pave the way for the development of novel RTP systems for versatile optoelectronic applications.

Introduction

https://doi.org/10.26434/chemrxiv-2024-hqwbs **ORCID:** https://orcid.org/0009-0009-6810-7086 Content not peer-reviewed by ChemRxiv. **License:** CC BY 4.0

The development of purely organic phosphorescent materials has garnered significant attention in scientific research due to their ability to exhibit high internal quantum efficiency, long exciton lifetime, and multiple stimulus response.[1-6] Despite its merits, molecular thermal motion can quench phosphorescence from the triplet states, limiting conventional purely organic compounds to only exhibit phosphorescence at cryogenic temperatures.[7] To overcome this limitation, several different approaches have been explored to enhance intersystem crossing (ISC) to realize room temperature phosphorescence (RTP) emission in pure organic materials, such as molecular aggregation,[8] incorporation of heavy atoms,[9] utilization of sensitizers,[10] or suppression nonradiative decay through crystallization,[11] matrix rigidification,[12] and supramolecular self-assembly.[13-14] In contrast, phosphorescence of isolated RTP molecules in dissolved solution (particularly in aerated solution) is unlikely to be observed, because of the significant molecular free volume with strong intramolecular motion, and great probability of diffusional collisions with quenchers (primarily oxygen).[15] This can be attributed to the following reasons (Fig. 1a): 1) isolated RTP molecules with weak intermolecular interactions, large singlet and triplet gap (ΔE_{ST}), and inefficient ISC and radiative decay hinder phosphorescence emission;[8] 2) conventional RTP molecules typically exhibit a low triplet level, which undergoes strong non-radiative processes in accordance with the energy gap law;[16] 3) most of them lack the ability to shield the chromophores from external quenchers, contributing to easy quenching of phosphorescence.[17] Therefore, these non-emissive RTP properties in solution make RTP materials difficult to meet the needs of optoelectronic devices,[18] information anti-counterfeiting,[19] biomedical imaging,[20] phosphorescence probes,[21] biosensing[22] and other fields.

Intrinsic RTP emitters possess inherent characteristics such as efficient ISC, strong triplet radiative transition, and low nonradiative decay. These attributes enable RTP to be observed without depending on the robust molecular environment, thus making phosphorescence in solution possible.[23-25] Furthermore, intrinsic RTP properties can be promoted and amplified by molecular aggregation due to the more energy splitting and ISC channels, more rigidified structures, and avoidable triplet exciton quenching.[26] Consequently, the rational design of intrinsic RTP materials is expected to achieve efficient phosphorescence in both solution and solid state. Dendrimers, highly branched macromolecules, are expected to become promising candidates for efficient intrinsic RTP materials because of their regulable triplet energy levels and characteristics, protective bulky peripheral dendrons and excellent processability and stability in various environments.[27-34] However, due to the high complexity and difficulty of synthesis, the use of dendronization strategies to achieve efficient intrinsic RTP dendrimers largely remains unexplored.

Therefore, up to this stage, we propose a design strategy aimed at achieving efficient intrinsic RTP molecules through dendronization. Our approach involves utilizing a donor-acceptor structure as an emitting center and dendrons as triplet regulators to facilitate conversion from thermally activated delayed fluorescence (TADF)[35-36] to

https://doi.org/10.26434/chemrxiv-2024-hqwbs **ORCID:** https://orcid.org/0009-0009-6810-7086 Content not peer-reviewed by ChemRxiv. **License:** CC BY 4.0

intrinsic RTP, as illustrated in Fig. 1b. The introduction of dendrons not only serves the dual purpose of maintaining a very small ΔE_{ST} and generating a higher population of triplets, thereby facilitating a multichannel ISC process but also effectively modulates the transition between different mixtures of charge transfer (CT) and localized (LE) states, resulting in an increased spin-orbit coupling (SOC) and enhanced ISC process and triplet radiation transition. Notably, the intrinsic RTP emission is observed in air-equilibrated solutions of the dendrimers, exhibiting phosphorescence lifetimes in the millisecond range. Moreover, the phosphorescence lifetimes are further prolonged with increasing aggregation degrees, showcasing aggregation-induced phosphorescence enhancement (AIPE)[37-38] behaviors. Additionally, the incorporation of these dendrimers into rigid polymer doped films leads to the manifestation of anti-Kasha dual phosphorescence emissions through triplet up-conversion.[39] Remarkably, amorphous films doped with the dendrimers as guests exhibit a high photoluminescence quantum yield (PLQY) of 98%, while the solution-processed organic light-emitting diodes (OLEDs) achieve an impressive external quantum efficiency (EQE) of 25.1%. These remarkable results firstly validate the effectiveness of dendrons regulated triplet design strategy in overcoming the limitations of previous RTP emitters. Moreover, the design rules established in this study can be extended to other chromophores, which open novel and inspiring possibilities for fine-tuning essential photophysical properties for applications.

Molecular design and solution photophysical properties

https://doi.org/10.26434/chemrxiv-2024-hqwbs **ORCID:** https://orcid.org/0009-0009-6810-7086 Content not peer-reviewed by ChemRxiv. **License:** CC BY 4.0

Our search for highly efficient intrinsic RTP dendrimers commenced with the selection of benzophenone (BP) as the donor and spiro[acridine-9,9’-fluorene] (SF) as the acceptor.[40] To effectively control the generation of triplet excitons, we introduced conjugated dendrons 1,3,5-tris(3',6'-di-*tert*-butyl-9*H*-[3,9'-bicarbazol]-9-yl)benzene (TC) and non-conjugated dendrons 1,3,5-tris(2-((6-(3,6-di-*tert*-butyl-9*H*-carbazol-9-yl)hexyl)oxy)-9*H*-carbazol-9-yl)benzene (HC) as triplet regulators. The design concept is illustrated in Fig. 2a. The synthetic routes and fundamental characterizations can be found in Supplementary Scheme 1 and Figs.1-2&43-59. By employing weak donating dendrons, we aimed to maintain a minimal overlap between the highest occupied molecular orbitals (HOMOs) and the lowest unoccupied molecular orbitals (LUMOs), as well as a narrow energy gap between singlet and triplet (ΔE_{ST}). This strategic approach effectively regulated the population of triplet excitons by increasing the triplet-triplet density and promoting a higher proportion of LE characteristics in the lowest triplet (T_1) state. These two factors were anticipated to enhance ISC processes from the lowest singlet (S_1) to T_1 and from the T_1 back to the ground state (S_0), thus facilitating efficient radiative transitions of triplet excitons and ultimately achieving highly efficient intrinsic RTP.

The ultraviolet–visible absorption spectra (Fig. 2a) reveal the presence of an intramolecular charge-transfer band spanning approximately 350 to 400 nm. The extinction coefficient shows an increase from around 8×10^3 M^{-1} cm^{-1} at 350 nm to approximately 6×10^4 M^{-1} cm^{-1} for the higher-lying localized absorption bands. In the photoluminescence (PL) spectra, TCBPSF and HCBPSF exhibit a sky-blue emission peak centered at 494 nm. However, HCBPSF also displays a blue fluorescence band originating from the TCzHCz unit, spanning a range of approximately 360 to 420 nm. This indicates that the HC unit does not participate in intramolecular charge transfer in dilute solution (Supplementary Fig.3). In the phosphorescence (Phos) spectra with a delayed time of 0.1 ms, TCBPSF exhibits a structureless CT-type emission, while HCBPSF demonstrates a partly resolved LE-type emission. The energy gap between singlet and triplet (ΔE_{ST}) are calculated at 0.05 and 0.02 eV for TCBPSF and HCBPSF at 298 K, respectively (Supplementary Figs. 4-5), suggesting that the long-lived emission spectra may originate from triplet states. In the transient PL decay spectra in solution (Fig. 2c), HCBPSF displays a significant long-lived lifetime with τ_P of 8.97 ms in air-equilibrated toluene. The lifetimes of the long-lived components decrease monotonically with increasing temperature, which is contrary to TADF[35-36] and consistent with phosphorescence[5-7] (Fig. 2d). Surprisingly, phosphorescence lifetimes with τ_P values of 1.13 ms are also observed in air-saturated solution (Fig. 2e). Additionally, TCBPSF exhibits a lifetime with τ_P values of 1.85 and 0.51 ms in air-equilibrated and air-saturated toluene, respectively (Supplementary Figs. 6-7). These dendrimers exhibit short-delayed fluorescence in toluene with low proportions (Supplementary Fig. 8). Furthermore, the presence of long phosphorescence is observed in various solutions of these dendrimers (Supplementary Figs. 9-10). These

https://doi.org/10.26434/chemrxiv-2024-hqwbs **ORCID:** https://orcid.org/0009-0009-6810-7086 Content not peer-reviewed by ChemRxiv. **License:** CC BY 4.0

results indicate that the intrinsic RTP exhibited by the dendrimers remains highly stable even in the presence of oxygen when dissolved in solution.

In solution, the quenching of triplet states by oxygen occurs through Dexter energy transfer, with the efficiency negatively correlated with the energy gap and positively correlated with the distance between donors and acceptors.[41] Interestingly, the dendrimers under investigation exhibit significantly higher T_1 levels of 2.86 and 2.89 eV compared with excited singlet oxygen ($^1O_2$) of 0.97 eV, indicating an unfavorable quenching efficiency by oxygen. To gain further insights into the involvement of oxygen in the triplet quenching process, we measured the reactive oxygen species (ROS) generation for the three molecules under UV irradiation, employing 9,10-anthracenediyl-bis(methylene)dimalonic acid (ABDA) as a singlet oxygen ($^1O_2$) indicator (Fig. 2f, Supplementary Fig. 11). Under light irradiation, the absorbance peaks of ABDA exhibited gradual decreases in the presence of both dendrimers; however, BPSF displayed a rapid drop in ABDA absorption.[42] The observed results suggest that the triplet excitons generated by the dendrimers exhibit lower production of $^1O_2$, indicating that the larger molecular volumes resulting from the dendronization of the shell package (with diameter of 20.1, 35.8, and 40.0 Å for BPSF, TCBPSF, and HCBPSF, respectively) effectively isolate the oxygen and inhibit triplet exciton quenching (Supplementary Fig. 12). These findings serve as evidence that the implementation of air-stable intrinsic RTP has been successfully achieved in these dendrimers.

https://doi.org/10.26434/chemrxiv-2024-hqwbs **ORCID:** https://orcid.org/0009-0009-6810-7086 Content not peer-reviewed by ChemRxiv. **License:** CC BY 4.0

To investigate the properties of intrinsic RTP from solution to aggregates, the PL properties of dendrimers in dilute THF/water solution were measured. The PL intensity of HCBPSF exhibited a steady decrease with adding water to fractions (f_w) of 60%, indicating the twisted intramolecular charge transfer (TICT) property. However, as the f_w increased to 90%, the PL emissions increased significantly by orders of magnitude, indicating a pronounced aggregation-induced emission[37] phenomenon (Supplementary Fig. 13). Concurrently, the PL lifetimes also exhibited a substantial increase from 3.2 to 28.0 ms with an increasing degree of aggregation (Fig. 3g), indicating AIPE[38] behaviors. Similar trends were observed in the THF/water solution of TCBPSF (Supplementary Fig. 13). The k_{nr} of TCBPSF and HCBPSF, respectively were calculated to be 547 and 314 s^{-1} in the 10% water solution, and significantly decreased to k_{nr} of 43 and 34 s^{-1} in the aggregated state with 90% water (Supplementary Figs. 14-17&Table S1-3), indicating restricted intramolecular motions and the blocking of nonradiative pathways with the degree of aggregation increases. These findings highlight the crucial role of aggregated states in promoting and amplifying the intrinsic RTP properties of the dendrimers, indicating their promising application prospects in aggregate states.

Quantum-chemical calculations

To gain a deeper insight into the fundamental basis of the intrinsic RTP exhibited by the dendrimer, quantum-chemical calculations were conducted to investigate two crucial photophysical processes:[25] (1) the enhancement of ISC spin-flipping processes from the S_1 to the nth triplet state (T_n) (k_{ISC}), and (2) the facilitation of the phosphorescent decay rate from the T_1 to the S_0 (k_P). The ISC process was evaluated based on equation (1)[24].

$$k_{ISC} \propto \sum_n \left|\langle S_1 | \hat{H}_{SOC} | T_n \rangle\right|^2 \exp(-E^2_{S_1T_n}) \tag{1}$$

Where smaller ΔE_{ST}, coupled with an increased number of ISC channels and larger spin-orbit coupling operator ($\hat{H}_{SOC}$) can enhance the ISC rate. Firstly, the dendronization strategy was found to preserve a small overlap between HOMOs and LUMOs, located on the donor and acceptor moieties, respectively (Supplementary Fig. 18), resulting in a very small ΔE_{ST} (0.02 and 0.14 eV), which is favorable for the ISC process. Secondly, the introduction of dendrons reduces the triplet-triplet energy gaps (ΔE_{TT}) and increases the density of triplet states, which promotes ISC channels from S_1 to T_n. Specifically, the dendronization of BPSF leads to the introduction of valid ISC channels with both small ΔE_{ST} ($\leq$ 0.37 eV) and high SOC values ($\geq$ 0.3 cm^{-1}).[43] As a result, the number of valid ISC routes increases from two to four, enabling the isolated dendrimer to exhibit intrinsic RTP. Thirdly, within the central-field approximation, when the spin of an electron is flipped over, $\hat{H}_{SOC}$ either suppresses or reinforces π-conjugation, leading to differing extents of π-conjugation.[44] Consequently, the SOC matrix element values for ISC can be qualitatively estimated by evaluating the changes in π-conjugation within the hole or electron wave functions between the singlet and triplet excited states. In Fig. 3d,[45] dendronization with different dendrons result in a

https://doi.org/10.26434/chemrxiv-2024-hqwbs **ORCID:** https://orcid.org/0009-0009-6810-7086 Content not peer-reviewed by ChemRxiv. **License:** CC BY 4.0

rotation of the dihedral angle between the donor and acceptor from 89.7° to 98.7° and 74.4°. This increased planarization causes the nature of T_1 to shift from CT states of BPSF shift to the hybridized local charge transfer (HLCT) state of TCBPSF and then to LE states of HCBPSF, thereby increasing the variation in the CT transition due to increasing the variation of CT transition between S_1 and T_1 ($\Delta CT_{ST}\%$) and the hole-electron overlap from 2.7% to 38.4% and 69.2%. Consequently, this significant increase in the SOC (S_1, T_1) constant from 0.13 to 0.42 and 0.66 cm^{-1} enhances the radiative transition of the triplet state. In summary, the introduction of dendron moieties effectively modulates the electronic structure of the excited state, incorporating a diverse mixture of CT and LE transitions, thereby enhancing the radiative decay of the triplet state.

In addition to achieving efficient ISC, another crucial factor for enhancing phosphorescence is increasing the k_P. The k_P is primarily determined by the transition dipole moment between the T_1 and S_0 states ($\mu_{T_1\to S_0}$), which can be expressed as equation (2,3).[25]

$$k_P = \frac{64\pi^4}{3\hbar^4 c^2}\Delta E^3_{T_1\to S_0}\left|\mu_{T_1\to S_0}\right|^2 \tag{2}$$

$$\mu_{T_1\to S_0} = \sum\nolimits_n \frac{\left\langle T_1\middle|\widehat{H}_{SOC}\middle|S_n\right\rangle}{{}^3E_1 - {}^1E_n} \times \mu_{S_n\to S_0} + \sum\nolimits_n \frac{\left\langle T_n\middle|\widehat{H}_{SOC}\middle|S_0\right\rangle}{{}^3E_n - {}^1E_0} \times \mu_{T_n\to T_1} \tag{3}$$

Where a larger SOC (S_1, T_n) by dendronization can increase the first term of equation (3) and promote $\mu_{T_1\to S_0}$ and k_P. By focusing on the second term of equation (3), dendronization increases the density of triplets and generates more energetically adjacent T_n states, which enhances the number of valid internal conversion processes

https://doi.org/10.26434/chemrxiv-2024-hqwbs **ORCID:** https://orcid.org/0009-0009-6810-7086 Content not peer-reviewed by ChemRxiv. **License:** CC BY 4.0

from T_n→T_1. Consequently, a high $\mu_{T_1 \to S_0}$ can be achieved by borrowing more on the intensity of spin-allowed T_n→T_1 transitions. Therefore, increasing triplet density by dendronization presents a viable approach to augment $\mu_{T_1 \to S_0}$. As a result, the $\mu_{T_1 \to S_0}$ increase from 1.09×10^{-6} to 2.90×10^{-5} and 3.06×10^{-5} D after dendronization. This significant increase indicates a considerably stronger phosphorescence emission can be anticipated in the dendrimer system.

Hence, the application of the dendronization strategy holds the potential to convert TADF into efficient intrinsic RTP by enhancing both the k_{ISC} and k_p achieved through the modulation of triplet energy levels and characteristics. To investigate the universality of this strategy, we conducted calculations on the excited states of various systems, including conjugated dendrimers TCBPAc and TCBPTZ, nonconjugated dendrimers HCBPAc and HCBPTZ, as well as TADF molecules BPAc and BPTZ (Supplementary Figs. 19-25). Our findings revealed that dendronization also leads to an increase in the ISC pathways, $\mu_{T_1 \to S_0}$, and SOC between T_1 and S_1/S_0 states. Consequently, these dendrimers are anticipated to exhibit efficient intrinsic RTP. These results provide strong evidence supporting the universality of the dendronization strategy.

Photoluminescence properties in polymer films

To investigate the RTP mechanisms of dendrimers in amorphous films, we systematically examined doped rigid polymer matrix films. In Fig. 4a, the Phos

https://doi.org/10.26434/chemrxiv-2024-hqwbs **ORCID:** https://orcid.org/0009-0009-6810-7086 Content not peer-reviewed by ChemRxiv. **License:** CC BY 4.0

spectrum of the PMMA: 1 wt% TCBPSF film exhibited a blue shift compared to the PL spectrum at 298K. Notably, an apparent negative ΔE_{ST} of -0.05 eV was observed. Time-resolved spectra (Fig. 4b) revealed dual phosphorescence emission peaks at 446 and 480 nm. The relative emission intensity at 446 nm gradually increased from 0.3 to 6 ms compared to the emission at 480 nm. This behavior can be attributed to a longer phosphorescence lifetime (Fig. 4c), suggesting that the emission at 446 nm may arise from a T_2 radiative transition, possibly resulting from an additional up-conversion process from the T_1 to T_2 state.[39] To validate these photophysical processes, we measured temperature-dependent phosphorescence spectra (Fig. 4d), which exhibited a monotonically blue shift from 504 to 477 nm as the temperature increased from 78 to 298 K. This observation suggests that elevated temperature promotes the endothermic up-conversion process from T_1 to T_2, with a small ΔE_{TT} of 0.2 eV, leading to the emission of anti-Kasha phosphorescence (Supplementary Figs. 26-29). The presence of a rigid polymer matrix facilitates the dual-phosphorescence processes by mitigating the influence of intermolecular interactions between emitters.[39] Additionally, the rigid environment provided by the matrix helps suppress nonradiative decay, thereby stabilizing the higher triplet state of the RTP dendrimers.[6] Similar dual-phosphorescence emission behavior was observed in doped rigid polycaprolactone (PCL) films, but not in doped soft poly(styrene-butadiene-styrene) (SBS) films (Supplementary Figs. 30-31).

https://doi.org/10.26434/chemrxiv-2024-hqwbs **ORCID:** https://orcid.org/0009-0009-6810-7086 Content not peer-reviewed by ChemRxiv. **License:** CC BY 4.0

The phosphorescence properties of HCBPSF in doped PMMA films were investigated. The PL and Ph spectra (Fig. 4e) of PMMA: 1 wt% HCBPSF film exhibited a positive ΔE_{ST} of 0.02 eV, indicating the presence of a stable ^{3}LE state at various temperatures, as confirmed by structure-resolved spectra (Supplementary Fig. 32). The films displayed an ultralong phosphorescence lifetime of 1.16 s, with persistent afterglow emission lasting up to 10 s in 298K. Interestingly, the lifetime of the triplet state excitons remained relatively unchanged across different temperatures. The PMMA matrix effectively restricted the mobility of the alkoxy chains in HCBPSF, thereby protecting triplet excitons from quenching and stabilizing the T_1 state, which ultimately resulted in extended triplet state exciton lifetimes, enabling ultralong RTP emission.[7] We also demonstrated a simple information anti-counterfeiting application (Fig. 4f) employing neat films and doped PMMA films. The number “88” exhibited sky-blue emission under UV light excitation. When the UV light was turned off, the portion of the number "8" written with the neat film disappeared due to its short-lived fluorescence, while the remaining portion exhibited afterglow phosphorescence, transforming into a new number "8" after 10 s. Furthermore, we investigated the transient PL decay of HCBPSF in doped PCL and SBS films (Supplementary Fig. 33). The different afterglow emission lifetimes observed in these doped films make them promising candidates for advanced encryption applications utilizing time-gated technology.

To elucidate the relationship between phosphorescence properties, molecular geometry, and the energetic ordering of triplet states, the $\Delta CT_{ST}\%$ between S_1 and T_1/T_2

https://doi.org/10.26434/chemrxiv-2024-hqwbs **ORCID:** https://orcid.org/0009-0009-6810-7086 Content not peer-reviewed by ChemRxiv. **License:** CC BY 4.0

and SOC elements between S_1/S_0 and T_1/T_2 were calculated (Fig. 4g, Supplementary Fig. 34). In the case of BPSF, the T_2 exhibits dominate ^{3}LE character with ΔCT_{ST} of 92.6% and acts as an intermediate state that facilitates strong vibronic coupling between ^{3}LE and ^{3}CT, and then facilitate the spin flipping process and TADF emission.[44] For TCBPSF (Fig. 4h), the presence of attached dendrons influences the dihedral angle and alters the characteristics of the triplet states, causing the ^{3}CT state to shift upwards and the ^{3}LE state to shift downwards. Consequently, the T_1 and T_2 states exhibit a mixed CT and LE character (^{3}HLCT), with similar SOC values (S_0, T_1) of 17.3 and 15.6 cm^{-1}. This suggests the possibility of the up-converted anti-Kasha dual phosphorescence in a rigid environment. In the case of HCBPSF (Fig. 4i), the dendrons regulate the dendrimer structures, resulting in a more planarized conjugated configuration that further elevates the energy of ^{3}CT and lowers the energy of ^{3}LE state. As a result, the T_1 predominantly exhibits the ^{3}LE state, while T_2 represents the ^{3}CT state with a small SOC (S_0, T_1) of 3.27 cm^{-1}. Consequently, T_1 becomes highly stable and emits afterglow phosphorescence in a rigid matrix. These findings indicate that the introduction of dendrons effectively modulates the electronic structure of the excited state, leading to different combinations of CT and LE transitions and, subsequently, diverse emission properties.

Photophysical properties of host doped films and OLED devices properties

Their PL and Ph spectra of the doped host 10-(4-((4-(9H-carbazol-9-yl)phenyl)sulfonyl)phenyl)-9,9-dimethyl-9,10-dihydroacridine (CzAcSF)[46] at 10 wt%

https://doi.org/10.26434/chemrxiv-2024-hqwbs **ORCID:** https://orcid.org/0009-0009-6810-7086 Content not peer-reviewed by ChemRxiv. **License:** CC BY 4.0

in films exhibit PL emissions at 481 and 478 nm, and phosphorescence emission at 483 and 482 nm for TCBPSF and HCBPSF, respectively, with small ΔE_{ST} of 0.02 eV at room temperature (Supplementary Figs. 35-39). The temperature-dependent phosphorescence and delayed fluorescence transition decays reveal three types of emissions: fluorescence, delayed fluorescence, and phosphorescence, accounting for 19.5%, 25.7% and 54.8%, respectively, for TCBPSF (Supplementary Table S4). In the doped films of HCBPSF, the corresponding proportions are 20.0%, 21.1% and 58.9%, respectively. The results of exciton dynamics demonstrate that the dendrimers exhibit smaller k_{RISC} and k_F of the dendrimers compared with TADF molecular BPSF, indicating a lower probability of emitting fluorescence and delayed fluorescence for the dendrimers. Moreover, the k_{ISC} of BPSF is significantly enhanced from 1.4×10^6 s^{-1} to 2.07×10^7 and 3.39×10^7 s^{-1} for TCBPSF and HCBPSF, respectively, resulting in a high k_P of 36.0 and 11.4 s^{-1}, which indicates the successful enhancement of intrinsic RTP emission through the dendronized strategy. In addition, compared with other RTP films,[18] the k_{nr} of the two dendrimers is remarkably low at 31.1 and 15.5 s^{-1}. Consequently, the PLQYs of TCBPSF and HCBPSF doped films reach up to 98% and 72%, respectively, highlighting their significant potential for the fabrication of efficient RTP-OLEDs.

In the realm of RTP OLEDs, several significant challenges persist, hindering their advancement.[47-50] These obstacles include the low PLQY in amorphous films, inferior EQE of the devices, unstable electroluminescence spectra and limited molecular design

https://doi.org/10.26434/chemrxiv-2024-hqwbs **ORCID:** https://orcid.org/0009-0009-6810-7086 Content not peer-reviewed by ChemRxiv. **License:** CC BY 4.0

strategy. These factors collectively impede the development of efficient and color-stable RTP-OLEDs. In this work, the RTP-OLED devices were fabricated by solution processing with a configuration of indium tin oxide (ITO)/poly(3,4-ethylenedioxythiophene): poly(styrenesulfonate) (PEDOT:PSS) (70 nm)/10-(4-((4-(9H-carbazol-9-yl)phenyl)sulfonyl)phenyl)-9,9-dimethyl-9,10-dihydroacridine (CzAcSF): emitters (90: 10, EML, 40 nm) /Bis[2-(diphenylphosphino)phenyl] ether oxide (DPEPO) (10 nm)/1,3,5-tri(m-pyrid-3-ylphenyl)benzene (TmPyPB) (50 nm)/ lithium fluoride (LiF) (1 nm)/ aluminum (Al) (100 nm) (Fig. 5a). Detailed device data are shown in Fig. 5b, c&d, and in Table 1. The fabricated devices exhibited sky-blue electroluminescence (EL) with a peak wavelength of 492 nm with the CIE color coordinates of (0.19, 0.36) and (0.18, 0.36), respectively. These values were slightly red-shifted compared with the PL spectra in doped films. Notably, the EL spectra remained remarkably stable at different voltages, owing to the small ΔE_{ST} and near-complete overlap of fluorescence and phosphorescence spectra (Supplementary Fig. 40). This achievement overcomes the limitations typically associated with conventional RTP devices.[18] The devices based on TCBPSF achieved higher maximum current efficiency (CE) of 59.5 cd/A, maximum power efficiency (PE) of 33.9 lm/W, and EQE_{max} of 25.1%. In contrast, the HCBPSF-based devices demonstrated CE_{max} of 38.6 cd/A, PE_{max} of 20.2 lm/W, and EQE_{max} of 17.2%, respectively. Supplementary Figs. 41-42 and Table S5-6 provide further information on devices with different structures. Considering that the light out-coupling efficiency of the conventional

OLEDs is 20-30%, the above-mentioned devices can achieve almost a unit exciton utilization rate. Hence, our design strategy, introducing dendrons to generate efficient intrinsic RTP, exhibits the significant potential to enhance the efficiency of RTP-OLEDs.

Conclusions

By employing newly developed dendronization strategy, we have successfully resolved a series of long-standing grand challenges, including the lack of intrinsic RTP in ambient solution, the absence of RTP dendrimers, inefficient RTP films and OLEDs, and the scarcity of anti-Kasha dual RTP materials. This breakthrough was made possible by incorporating dendronized TADF small molecules into small ΔE_{TT} and large ^{3}LE characteristics, which enhanced their SOC, ISC process and $\mu_{T_1 \to S_0}$, leading to efficient RTP emissions. Furthermore, computational studies on similar dendrimers yielded analogous results, verifying the generality of our strategy. Moreover, precise control over triplet energy gaps, densities, and characteristics plays crucial part in achieving highly efficient intrinsic RTP emissions, which will offer guidance for molecular design in the field of phosphorescent materials. Consequently, our research contributes to a deep understanding of how to regulate excited states in molecular systems to achieve efficient intrinsic RTP and opens new perspectives for the development of advanced materials in the field of optoelectronics.

https://doi.org/10.26434/chemrxiv-2024-hqwbs **ORCID:** https://orcid.org/0009-0009-6810-7086 Content not peer-reviewed by ChemRxiv. **License:** CC BY 4.0

Online content

Any reporting summaries, source data, extended data, supplementary information, acknowledgments, peer review information; details of author contributions and competing interests; and statements of data and code availability are available at https://doi.org/.

Methods

Materials

Unless otherwise noted, all the chemicals and reagents were obtained from commercial sources (J&K, TCI, Meryer or Sigma Aldrich). The solvents for reactions were distilled and degassed before use. All reactions were carried out in an N_2 atmosphere with a dried Schlenk glassware or tube. ^1H and ^{13}C nuclear magnetic resonance (NMR) spectra were measured using deuterated $CDCl_3$, DMSO-d_6 as solvent. on a Bruker AV 500 spectrometer or a Bruker AVIII 400 spectrometer at room temperature. High-resolution mass spectra (HRMS) were obtained on a GCT premier CAB048 mass spectrometer operating in a MALDI-TOF mode. HPLC measurements were carried out on a Waters 2487 (600E) equipment with column of Poroshell 120 (EC-C18, 2.7 m, 4.6 150 mm).

Characterization

UV-Vis absorption spectra were measured on a PerkinElmer Lambda 950 spectrophotometer. Photoluminescence (PL) spectra, transient PL decay spectra and photoluminescence quantum yields were performed on an Edinburgh FLS1000

https://doi.org/10.26434/chemrxiv-2024-hqwbs **ORCID:** https://orcid.org/0009-0009-6810-7086 Content not peer-reviewed by ChemRxiv. **License:** CC BY 4.0

fluorescence Spectrofluorometer. Cyclic voltammograms were measured in a solution of tetra-*n*-butylammonium hexafluorophosphate ($n\mathrm{Bu_4NPF_6}$, 0.1 M) in acetonitrile at a scan rate of 50 mV s^{-1}, using a platinum wire as the auxiliary electrode, a glass carbon disk as the working electrode, and Ag/Ag^+ as the reference electrode, standardized for the redox couple ferricenium/ferrocene (Fc/Fc^+) (HOMO = $-[E_{ox} + 4.8]$ eV, and LUMO = $-[E_{re} + 4.8]$ eV). E_{ox} and E_{re} represent the onset oxidation and reduction potentials relative to Fc/Fc^+, respectively. Thermogravimetric analysis (TGA) was carried out on TA TGA Q5000 under dry nitrogen at a heating rate of 10 °C min^{-1}. Thermal transition was investigated by TA DSC Q1000 under dry nitrogen at a heating rate of 10 °C min^{-1}.

Computational Details

The ground state geometries were optimized using the density functional theory (DFT) method with PBE0-D3 functional at the basis set level of 6-31G (d, p), and the excited-state geometries were optimized using the time-dependent DFT method with PBE0-D3 functional at the basis set level of 6-31G (d, p). The above calculations were performed using Gaussian16 package. The spin-orbital coupling constants were calculated based on PBE0/def2-SV(P) by using ORCA 5.0.2. The natural transition orbital analyses were analyzed with Multiwfn.

Device Fabrication and Characterization

The hole-injection material modified PEDOT:PSS (PEDOT:PSS-HJ-1, was purchased from Jinghang Optoelectronics (Shenzhen) Corporation and the electron transporting materials TmPyPB was obtained from Shanghai Xinrunsheng Corporation and used as received. The ITO-coated glass with a sheet resistance of 15 Ω per square was used as the substrate. Before device fabrication, the ITO-coated glass substrate was precleaned

https://doi.org/10.26434/chemrxiv-2024-hqwbs **ORCID:** https://orcid.org/0009-0009-6810-7086 Content not peer-reviewed by ChemRxiv. **License:** CC BY 4.0

and exposed to UV-ozone for 20 min. PEDOT:PSS was then spin-coated onto the clean ITO substrate as a hole-injection layer. Then, a solution of the emitter dissolved in chlorobenzene was spin-coated (10 mg/mL; 1000 rpm) to form a 40 nm-thick emissive layer and annealed at 50 °C for 30 min. Next, an exciton blocking layer of DPEPO with 10 nm thickness was vacuum deposited. Finally, a 50 nm-thick electron-transporting layer of TmPyPB was vacuum deposited, and a cathode composed of 1 nm-thick Liq and aluminum (100 nm) was deposited onto the substrate through shadow masking with a pressure of 10^{-6} Torr. The current density-voltage-luminance (J-V-L) characteristics of the devices were measured using a Keithley 2400 Source meter and a Spectroradiometer PhotoResearch PR735. The EL spectra were recorded simultaneously with PR735. The EQE values were calculated from the luminance, current density, and electroluminescence spectrum according to previously reported methods. All measurements were performed at room temperature under ambient conditions after device encapsulation with UV curable resin.

Data availability

All data are available in the main text or supplementary materials. The data and code that support the findings of this study are available from the corresponding authors on request.

Author contributions

C.L. designed the experiments and performed the synthesis, major theoretical calculations, and photophysical measurements. Z.L. and Z. L. performed the theoretical calculations. M.W., H.T., F.G., M.L., and S.G. performed photophysical measurements. G.X. and Y. M. characterized OLEDs. X.C., Z.Q., Z.Z., L.H., G.X., Z.R., Y.L., S.Y., R.K., J.L., D.M., and B.Z.T. took part in the discussion and gave important suggestions.

https://doi.org/10.26434/chemrxiv-2024-hqwbs **ORCID:** https://orcid.org/0009-0009-6810-7086 Content not peer-reviewed by ChemRxiv. **License:** CC BY 4.0

Z.X. and H.Z. co-wrote the paper. All authors approved the final version of the manuscript.

Competing interests

The authors declare no competing interests.

Acknowledgements

This work was supported by the National Natural Science Foundation of China Grant (52273197, 52333007, 22103062, 52373195 and 52273164); the Research Grants Council of Hong Kong (16304819, 16305320 and C6014-20W); the Innovation and Technology Commission (ITCCNERC14SC01); the Natural Science Foundation of Guangdong Province (2019B121205002 and 2019B030301003); the Shenzhen Key Laboratory of Functional Aggregate Materials (ZDSYS 20211021111400001); the Science, Technology and Innovation Commission of Shenzhen Municipality (GJHZ 20210705141810031, JCYJ 2021324134613038, KQTD 20210811090142053, GJHZ 20210705141810031); Shanghai Pujiang Program (No. 22PJ1402800); Shandong Provincial Natural Science Foundation (ZR2022ZD37); the Fundamental Research Funds for the Central Universities (QNTD20). The authors thank to the AIE Institute (www.aietech.org.cn) for providing some technical assistance and the Materials Characterization and Preparation Center, The Chinese University of Hong Kong, Shenzhen, for materials characterization.

https://doi.org/10.26434/chemrxiv-2024-hqwbs **ORCID:** https://orcid.org/0009-0009-6810-7086 Content not peer-reviewed by ChemRxiv. **License:** CC BY 4.0

References:

1. Zhang, G. et al. Multi-emissive difluoroboron dibenzoylmethane polylactide exhibiting intense fluorescence and oxygen-sensitive room-temperature phosphorescence. *J. Am. Chem. Soc.* 129, 8942–8943 (2007).
2. Bolton, O., Lee, K., Kim, H. J., Lin, K. Y. & Kim, J. Activating efficient phosphorescence from purely organic materials by crystal design. *Nat. Chem.* **3**, 205-210 (2011).
3. An, Z. et al. Stabilizing triplet excited states for ultralong organic phosphorescence. *Nat. Mater.* **14**, 685-690 (2015).
4. Gu, L. et al. Colour-tunable ultra-long organic phosphorescence of a single-component molecular crystal. *Nat. Photonics* **13**, 406-411 (2019).
5. Zhao, W., He, Z. & Tang, B. Z. Room-temperature phosphorescence from organic aggregates. *Nat. Rev. Mater.* **5**, 869-885 (2020).
6. Ye, W. *et al.* Confining isolated chromophores for highly efficient blue phosphorescence. *Nat. Mater.* **20**, 1539-1544 (2021).
7. Kenry, Chen, C. & Liu, B. Enhancing the performance of pure organic room-temperature phosphorescent luminophores. *Nat. Commun.* **10**, 2111 (2019).
8. Yang, L. *et al.* Aggregation-induced intersystem crossing: a novel strategy for efficient molecular phosphorescence. *Nanoscale* **8**, 17422-17426 (2016).
9. Yan, Z. A., Lin, X., Sun, S., Ma, X. & Tian, H. Activating Room-Temperature Phosphorescence of Organic Luminophores via External Heavy-Atom Effect and Rigidity of Ionic Polymer Matrix. *Angew. Chem. Int. Ed.* **60**, 19735-19739 (2021).
10. Kuila, S. & George, S. J. Phosphorescence Energy Transfer: Ambient Afterglow Fluorescence from Water-Processable and Purely Organic Dyes via Delayed Sensitization. *Angew. Chem. Int. Ed.* **59**, 9393-9397 (2020).
11. Yang, J. *et al.* The influence of the molecular packing on the room temperature phosphorescence of purely organic luminogens. *Nat. Commun.* **9**, 840 (2018).

https://doi.org/10.26434/chemrxiv-2024-hqwbs **ORCID:** https://orcid.org/0009-0009-6810-7086 Content not peer-reviewed by ChemRxiv. **License:** CC BY 4.0

12. Hamzehpoor, E. *et al.* Efficient room-temperature phosphorescence of covalent organic frameworks through covalent halogen doping. *Nat. Chem.* **15**, 83-90 (2022).

13. Ma, X., Wang, J. & Tian, H. Assembling-Induced Emission: An Efficient Approach for Amorphous Metal-Free Organic Emitting Materials with Room-Temperature Phosphorescence. *Acc. Chem. Res.* **52**, 738-748 (2019).

14. Ma, X. K. & Liu, Y. Supramolecular Purely Organic Room-Temperature Phosphorescence. *Acc. Chem. Res.* **54**, 3403-3414 (2021).

15. Sun, H. & Zhu, L. Achieving purely organic room temperature phosphorescence in aqueous solution. *Aggregate* **4**, e253 (2022).

16. Wei, Y.-C. *et al.* Overcoming the energy gap law in near-infrared OLEDs by exciton–vibration decoupling. *Nat. Photonics* **14**, 570-577 (2020).

17. Liu, D. *et al.* Molecular core–shell structure design: Facilitating delayed fluorescence in aggregates toward highly efficient solution-processed OLEDs. *Aggregate*, **3**, e164 (2022).

18. Zhou, Z. *et al.* Recent advances in metal-free phosphorescent materials for organic light-emitting diodes. *J. Mater. Chem. C* **11**, 3143-3161 (2023).

19. Wang, D. *et al.* Achieving Color-Tunable and Time-Dependent Organic Long Persistent Luminescence via Phosphorescence Energy Transfer for Advanced Anti-Counterfeiting. *Adv. Funct. Mater.* **33**, 2208895 (2023).

20. Zhang, Y. *et al.* Organic room-temperature phosphorescence materials for bioimaging. *Chem. Commun.* **59**, 5329-5342 (2023).

21. Zhen, X., Qu, R., Chen, W., Wu, W. & Jiang, X. The development of phosphorescent probes for in vitro and in vivo bioimaging. *Biomater. Sci.* **9**, 285-300 (2021).

22. DeRosa, C. A. *et al.* Oxygen Sensing Difluoroboron beta-Diketonate Polylactide Materials with Tunable Dynamic Ranges for Wound Imaging. *ACS Sens.* **1**, 1366-1373 (2016).

23. Zhao, W. *et al.* Rational Molecular Design for Achieving Persistent and Efficient Pure Organic Room-Temperature Phosphorescence. *Chem* **1**, 592-602 (2016).

https://doi.org/10.26434/chemrxiv-2024-hqwbs **ORCID:** https://orcid.org/0009-0009-6810-7086 Content not peer-reviewed by ChemRxiv. **License:** CC BY 4.0

24. Ma, H., Peng, Q., An, Z., Huang, W. & Shuai, Z. Efficient and Long-Lived Room-Temperature Organic Phosphorescence: Theoretical Descriptors for Molecular Designs. *J. Am. Chem. Soc.* **141**, 1010-1015 (2019).
25. Hirata, S. Recent Advances in Materials with Room-Temperature Phosphorescence: Photophysics for Triplet Exciton Stabilization. *Adv. Opt. Mater.* **5**, 1700116 (2017).
26. Peng, Q., Ma, H. & Shuai, Z. Theory of Long-Lived Room-Temperature Phosphorescence in Organic Aggregates. *Acc. Chem. Res*. **54**, 940-949 (2020).
27. Tomalia, D. A. *et al.* A New Class of Polymers: Starburst-Dendritic Macromolecules. *Polym. J.* **17**, 117-132 (1985).
28. Fréchet, J. M. J. Functional Polymers and Dendrimers: Reactivity, Molecular Architecture, and Interfacial Energy. *Science* **263**, 1710-1715 (1994).
29. Burn, P. L., Lo, S. C. & Samuel, I. D. W. The Development of Light-Emitting Dendrimers for Displays. *Adv. Mater.* **19**, 1675-1688 (2007).
30. Albrecht, K., Matsuoka, K., Fujita, K. & Yamamoto, K. Carbazole dendrimers as solution-processable thermally activated delayed-fluorescence materials. *Angew. Chem. Int. Ed.* **54**, 5677-5682 (2015).
31. Li, Y., Xie, G., Gong, S., Wu, K. & Yang, C. Dendronized delayed fluorescence emitters for non-doped, solution-processed organic light-emitting diodes with high efficiency and low efficiency roll-off simultaneously: two parallel emissive channels. *Chem. Sci.* **7**, 5441-5447 (2016).
32. Li, C. *et al.* Asymmetrical-Dendronized TADF Emitters for Efficient Non-doped Solution-Processed OLEDs by Eliminating Degenerate Excited States and Creating Solely Thermal Equilibrium Routes. *Angew. Chem. Int. Ed.* **134**, e202115140 (2021).
33. Li, C. *et al.* TADF Dendronized Polymer with Vibrationally Enhanced Direct Spin-Flip between Charge-Transfer States for Efficient Non-doped Solution-Processed OLEDs. *Chem. Eng. J.* **435**, 134924 (2022).

https://doi.org/10.26434/chemrxiv-2024-hqwbs **ORCID:** https://orcid.org/0009-0009-6810-7086 Content not peer-reviewed by ChemRxiv. **License:** CC BY 4.0

34. Wang, X. et al. pi-Stacked Donor-Acceptor Dendrimers for Highly Efficient White Electroluminescence. *Angew. Chem. Int. Ed.* **60**, 16585-16593 (2021).

35. Uoyama, H., Goushi, K., Shizu, K., Nomura, H. & Adachi, C. Highly efficient organic light-emitting diodes from delayed fluorescence. *Nature* **492**, 234-238 (2012).

36. Liu, Y., Li, C., Ren, Z., Yan, S. & Bryce, M. R. All-organic thermally activated delayed fluorescence materials for organic light-emitting diodes. *Nat. Rev. Mater.* **3**, 18020 (2018).

37. Zhao, Z., Zhang, H., Lam, J. W. Y. & Tang, B. Z. Aggregation-Induced Emission: New Vistas at the Aggregate Level. *Angew. Chem. Int. Ed.* **59**, 9888-9907 (2020).

38. Sathish, V., Ramdass, A., Thanasekaran, P., Lu, K.-L. & Rajagopal, S. Aggregation-induced phosphorescence enhancement (AIPE) based on transition metal complexes—An overview. *J. Photochem. Photobiol., C* **23**, 25-44 (2015).

39. Li, J. *et al.* A direct observation of up-converted room-temperature phosphorescence in an anti-Kasha dopant-matrix system. *Nat. Commun.* **14**, 1987 (2023).

40. Fu, Y. *et al.* Boosting external quantum efficiency to 38.6% of sky-blue delayed fluorescence molecules by optimizing horizontal dipole orientation. *Sci. Adv.* **7**, eabj2504 (2021).

41. Wilkinson, F. & Abdel-Shafi, A. A. Mechanism of Quenching of Triplet States by Oxygen: Biphenyl Derivatives in Acetonitrile. *J. Phys. Chem. A* **101**, 5509-5516 (1997).

42. Liu, S. et al. Cationization-Enhanced Type I and Type II ROS Generation for Photodynamic Treatment of Drug-Resistant Bacteria. *ACS Nano* **16**, 9130-9141 (2022).

43. Chen, R. *et al.* Promoting Singlet/triplet Exciton Transformation in Organic Optoelectronic Molecules: Role of Excited State Transition Configuration. *Sci. Rep.* **7**, 6225 (2017).

https://doi.org/10.26434/chemrxiv-2024-hqwbs **ORCID:** https://orcid.org/0009-0009-6810-7086 Content not peer-reviewed by ChemRxiv. **License:** CC BY 4.0

44. Samanta, P. K., Kim, D., Coropceanu, V. & Bredas, J. L. Up-Conversion Intersystem Crossing Rates in Organic Emitters for Thermally Activated Delayed Fluorescence: Impact of the Nature of Singlet vs Triplet Excited States. *J. Am. Chem. Soc.* **139**, 4042-4051 (2017).
45. Lu, T. & Chen, F. Multiwfn: a multifunctional wavefunction analyzer. *J. Comput. Chem.* **33**, 580-592 (2012).
46. Lee, D. R. *et al.* Design strategy for 25% external quantum efficiency in green and blue thermally activated delayed fluorescent devices. *Adv. Mater.* **27**, 5861-5867 (2015).
47. Chaudhuri, D. *et al.* Metal-free OLED triplet emitters by side-stepping Kasha's rule. *Angew. Chem. Int. Ed.* **52**, 13449-13452 (2013).
48. Wang, T. *et al.* Aggregation-induced dual-phosphorescence from organic molecules for nondoped light-emitting diodes. *Adv. Mater.* **31,** 1904273 (2019).
49. Liu, X. *et al.* An Electroactive Pure Organic Room-Temperature Phosphorescence Polymer Based on a Donor-Oxygen-Acceptor Geometry. *Angew. Chem. Int. Ed.* **60,** 2455-2463 (2021).
50. Chen, Z. *et al.* Highly Efficient Purely Organic Phosphorescence Light-Emitting Diodes Employing a Donor-Acceptor Skeleton with a Phenoxaselenine Donor. *Adv. Sci*. e2207003 (2023).

Figures in the main text

https://doi.org/10.26434/chemrxiv-2024-hqwbs **ORCID:** https://orcid.org/0009-0009-6810-7086 Content not peer-reviewed by ChemRxiv. **License:** CC BY 4.0

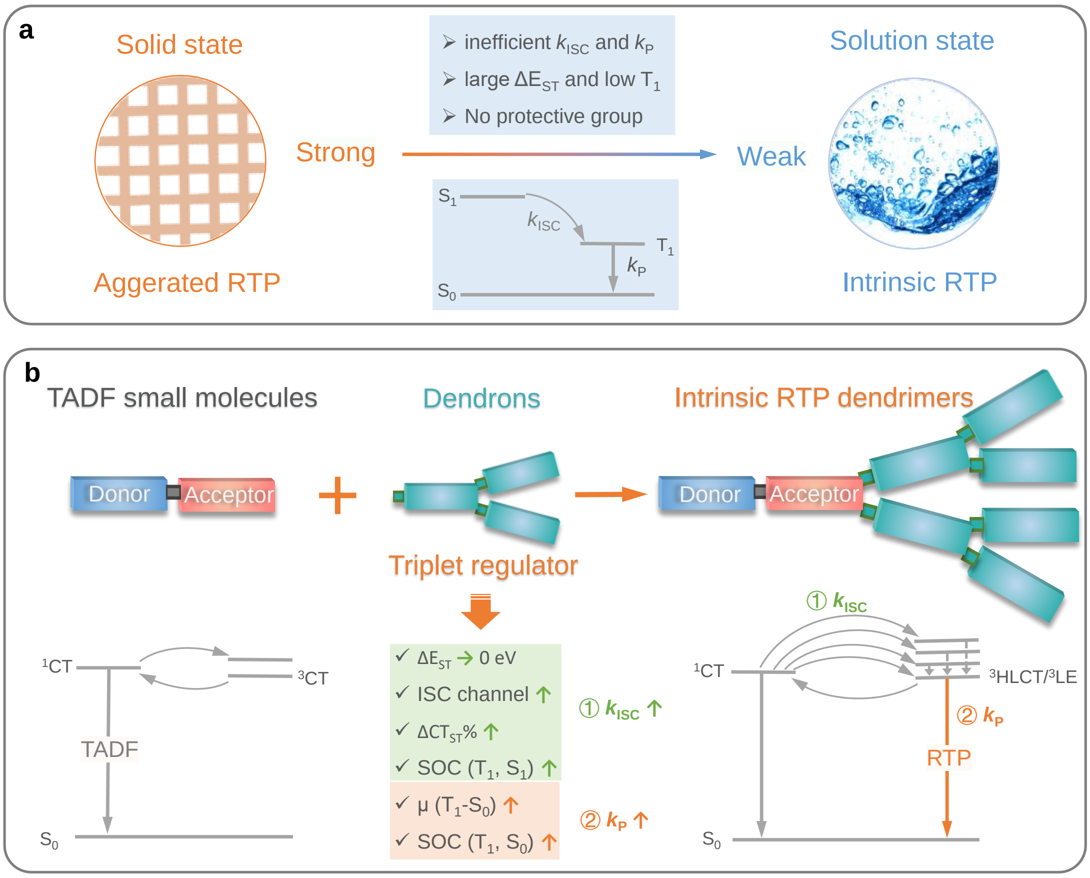

Fig. 1 | The mechanisms of aggregated RTP and intrinsic RTP. a, the properties of RTP in solid and solution state. As the solid and solution transition, the RTP performance decreases due to the inefficient k_{ISC} and k_P, large ΔE_{ST} and low T_1, and no protective group. **b**, Strategy to achieve efficient intrinsic RTP through incorporating dendrons. Molecular dendronization accomplishes concerted enhancement, such as keeping the very small ΔE_{ST} of ~0 eV, increasing ISC channel, and ΔCT_{ST}%, and SOC (T_1, S_1) and leading to improved k_{ISC}; enhanced μ(T_1-S_0) and SOC (T_1, S_0) and leading to k_P. ΔCT_{ST}% is the difference in CT distribution between singlet and triplet. SOC is spin-orbital coupling. μ is the transition dipole moment.

https://doi.org/10.26434/chemrxiv-2024-hqwbs **ORCID:** https://orcid.org/0009-0009-6810-7086 Content not peer-reviewed by ChemRxiv. **License:** CC BY 4.0

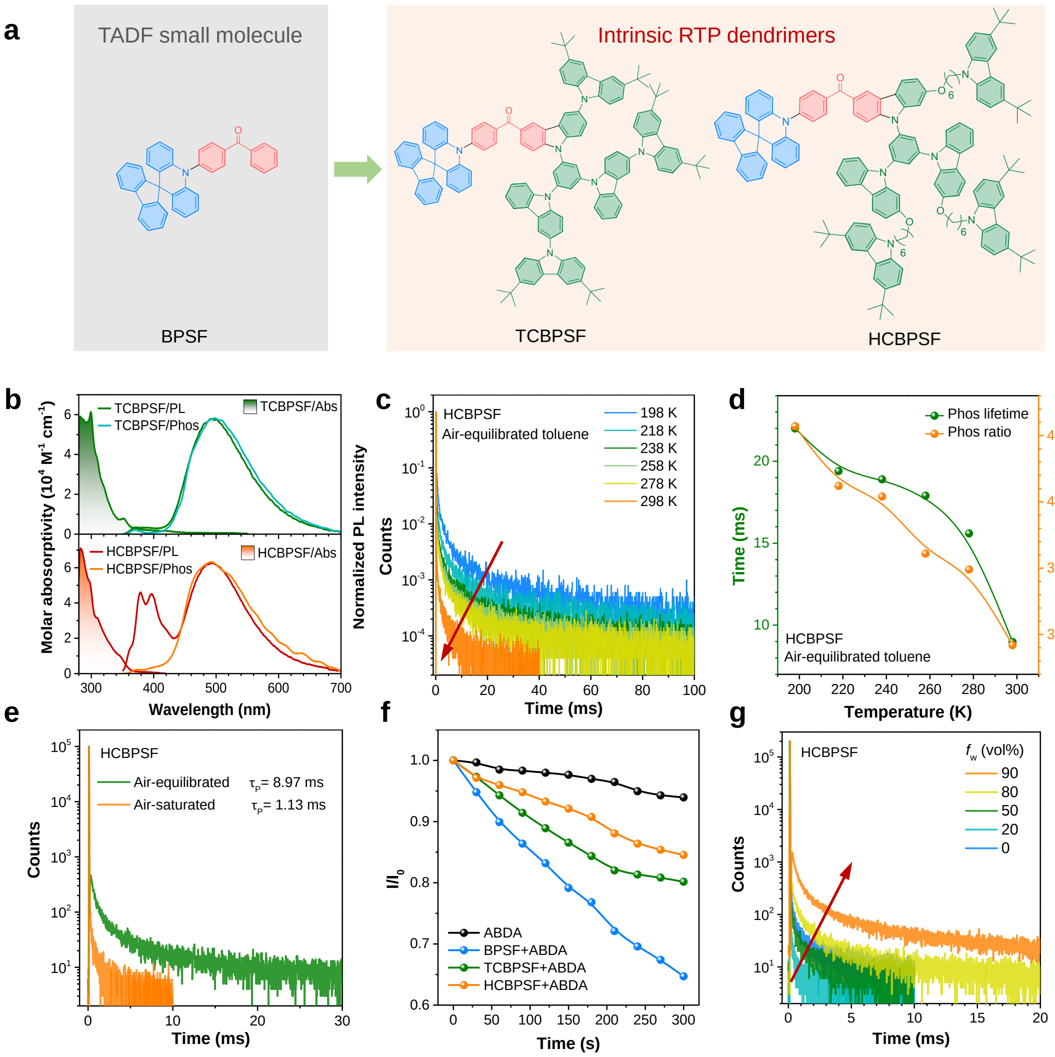

Fig. 2 | The molecular structures and their photophysics in solutions. a, The chemical structures of BPSF, TCBPSF, and HCBPSF. **b**, UV-vis absorption, PL spectra, and Phos spectra of TCBPSF and HCBPSF in air-equilibrated toluene solution. **c**, Temperature-dependent transient phosphorescence decay spectra of HCBPSF in toluene solution. **d**, The plots of lifetimes and proportions of phosphorescence of HCBPSF at different temperatures. **e**, The transient phosphorescence decay spectra of HCBPSF in air-equilibrated and air-saturated conditions. **f**, access of $^1O_2$ generation with the decomposition of ABDA for these BPSF, TCBPSF, and HCBPSF under light

https://doi.org/10.26434/chemrxiv-2024-hqwbs **ORCID:** https://orcid.org/0009-0009-6810-7086 Content not peer-reviewed by ChemRxiv. **License:** CC BY 4.0

irradiation. **g**, Transient PL decay spectra of HCBPSF in water/THF mixtures with different f_w.

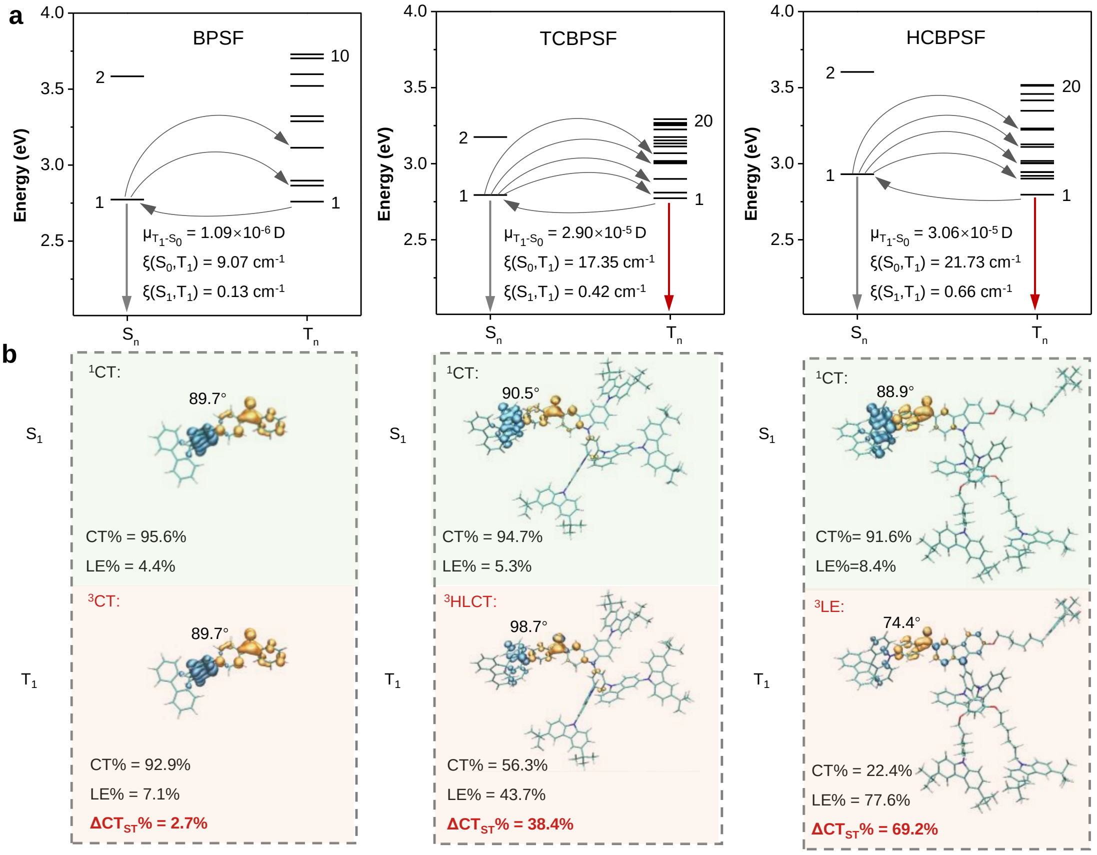

Fig. 3 | The excited states properties of the three compounds. a, The excited states, photophysical processes, triplet radiative transition ($\mu_{T_1 \to S_0}$), SOC constants of BPSF, TCBPSF, and HCBPSF. **b**, the hole and electron distribution and the CT and LE proportions of S_1 and T_1 of BPSF, TCBPSF, and HCBPSF. These angles are the dihedral angles between the donor and acceptor.

https://doi.org/10.26434/chemrxiv-2024-hqwbs **ORCID:** https://orcid.org/0009-0009-6810-7086 Content not peer-reviewed by ChemRxiv. **License:** CC BY 4.0

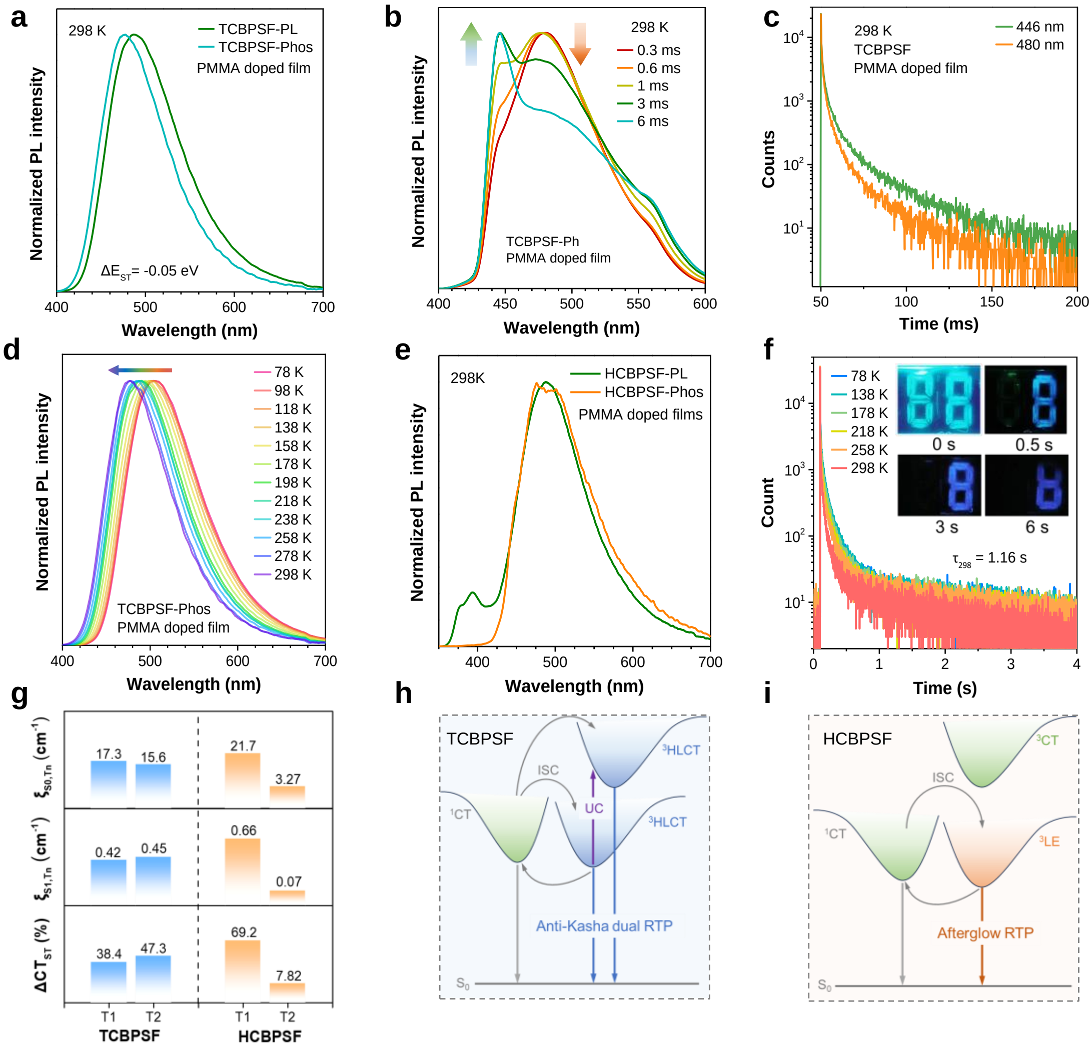

Fig. 4 | The photophysics of the RTP dendrimers in PMMA films. a, PL and Phos spectra of TCBPSF doped in PMMA films at 298K. **b**, Time-resolved PL spectra of TCBPSF doped in PMMA films at 298K. **c**, Transient PL decay spectra at 446 nm and 480 nm of TCBPSF doped in PMMA films. **d**, Temperature-dependent delayed PL spectra of HCBPSF in PMMA films from 78K to 298K. **e**, PL and Phos spectra of HCBPSF doped in PMMA films at 298K. **f**, Temperature-dependent transient PL decay spectra of HCBPSF in PMMA films from 78K to 298K. Inset: information encryption photographs by different afterglow times of neat films (left) and PMMA films (right) design based on HCBPSF at 298K. **g**, The $\Delta CT_{ST}\%$ of T_1 and T_2 states, SOCME (S_1,

https://doi.org/10.26434/chemrxiv-2024-hqwbs **ORCID:** https://orcid.org/0009-0009-6810-7086 Content not peer-reviewed by ChemRxiv. **License:** CC BY 4.0

T_n, n = 1, 2), and SOCME (S_0, T_n, n = 1, 2) of TCBPSF and HCBPSF. **h-i,** The photophysical processes of TCBPSF and HCBPSF in PMMA matrix, respectively. UC is a triplet-triplet up-conversion process.

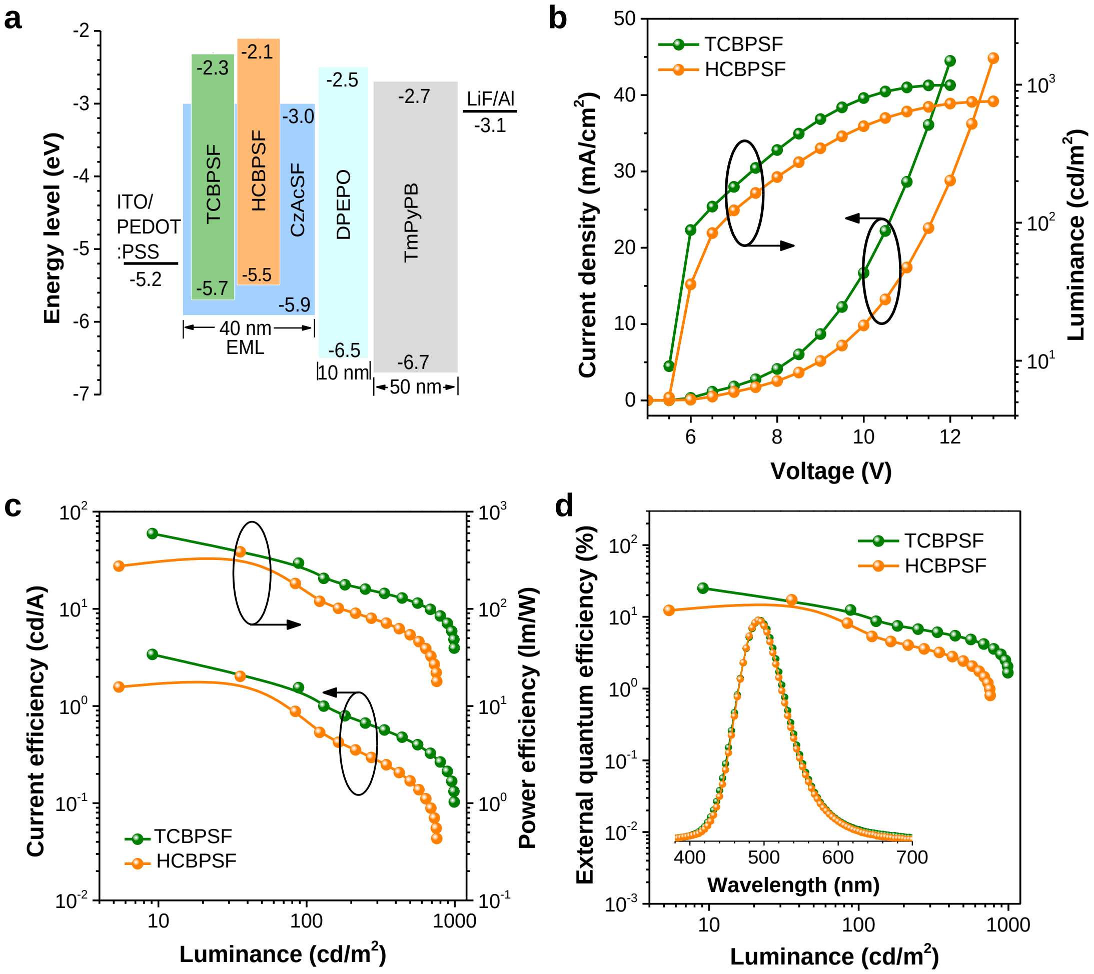

Fig. 5 | The properties of the solution-processed OLEDs based on the RTP dendrimers. a, Device structure with the energy-level diagrams. **b**, Current density-voltage-luminance curves of the devices. **c**, Current efficiency-luminance-power efficiency curves of the devices the devices. **d**, External quantum efficiency versus luminance curves of the devices. Inset: electroluminescence spectra of the devices.

Table 1 | EL properties of the solution-processed OLEDs

https://doi.org/10.26434/chemrxiv-2024-hqwbs **ORCID:** https://orcid.org/0009-0009-6810-7086 Content not peer-reviewed by ChemRxiv. **License:** CC BY 4.0

	V_{on}[a] (V)	L_{max}[b] (cd/m^2)	CE_{max}[c] (cd/A)	PE_{max}[d] (lm/W)	EQE_{max}[e] (%)	EL peak[f] (nm)	CIE[g] (x,y)
TCBPSF	5.5	991	59.5	33.9	25.1	492	0.19. 0.36
HCBPSF	5.5	757	38.6	20.2	17.2	492	0.18. 0.36

[a] Turn-on voltage at 1 cd/m^2. [b] Maximum luminance. [c] Maximum current efficiency. [d] Maximum power efficiency. [e] Maximum external quantum efficiency. [f] The peak value of electroluminescence. [g] Coordinates of Commission Internationale de l'éclairage.

https://doi.org/10.26434/chemrxiv-2024-hqwbs **ORCID:** https://orcid.org/0009-0009-6810-7086 Content not peer-reviewed by ChemRxiv. **License:** CC BY 4.0